THE JOURNAL OF PHYSICAL CHEMISTRY B

Article

pubs.acs.org/JPCB

Protein Secondary Structure Imaging with Ultrabroadband Multiplex Coherent Anti-Stokes Raman Scattering (CARS) Microspectroscopy

Kotatsu Bito,[†,‡] Masanari Okuno,[‡] Hideaki Kano,[‡] Shihomi Tokuhara,[†] Satoru Naito,[†] Yoshinori Masukawa,[†] Philippe Leproux,[§,∥] Vincent Couderc,[§] and Hiro-o Hamaguchi*[,‡,⊥]

[†]Analytical Science Research Laboratories, Kao Corporation, Akabane 2606, Ichikai, Haga, Tochigi 321-3497, Japan

[‡]Department of Chemistry, School of Science, The University of Tokyo, Hongo 7-3-1, Bunkyo, Tokyo 113-0033, Japan

[§]Institut de Recherche XLIM, UMR CNRS 6172, 123 Avenue Albert Thomas, 87060 Limoges Cedex, France

[∥]LEUKOS, ESTER Technopole, 1 Avenue d'Ester, 87069 Limoges Cedex, France

[⊥]Institute of Molecular Science and Department of Applied Chemistry, National Chiao Tung University, Ta Hsueh Road 1001, Hsinchu 300, Taiwan

ABSTRACT: Protein secondary structures in human hair have been studied with ultrabroadband multiplex coherent anti-Stokes Raman scattering (CARS) microspectroscopy. The CARS peak-shift mapping method has been developed and applied to hair samples with and without treatments by chemical reduction and mechanical extension. It clearly visualizes the treatment induced changes in protein secondary structures and their spatial distributions. Using the new imaging technique, we found a multilayered structure in the human hair cortex.

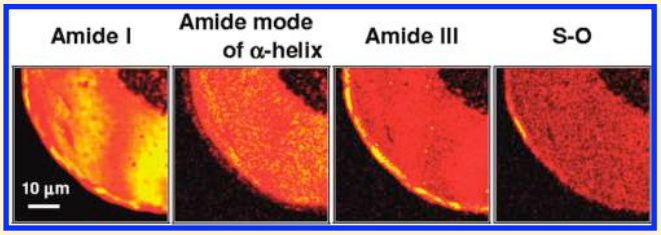

Properties of a protein are determined by its primary, secondary, and higher structures. The secondary structure regulates higher structures that determine protein functions. Hence, a number of analytical methods, X-ray diffraction,[1,2] circular dichroism,[3,4] NMR spectroscopy,[5,6] and vibrational spectroscopies[7−9] have been employed to determine the secondary structure of proteins. However, these methods lack in space specificity to elucidate the spatial inhomogeneity of protein secondary structures on micrometer scales.

Human hair is one of the most important model systems for investigating protein structures and their functions from the viewpoints of protein chemistry as well as polymer and cosmetic sciences.[10−12] A human hair is made of keratinous fibers (Figure 1), which consist of three main regions: the medulla (porous materials), cortex (fibrous materials), and cuticle (outer layer scales) regions from inside to outside. Although all of the three regions are composed of keratin proteins, keratin associated proteins (KAPs), and other proteins, their secondary structures are different from one another, reflecting different protein functions and properties. Control of their secondary structures is highly important for cosmetic science. Among the three regions, the cortex is the most important because it is the main part of the hair. The cortex consists of spindle-shaped macrofibrils that have two main structures, intermediate filament (IF) and KAPs (Figure 1). KAPs are composed mainly of globular proteins. The IFs and KAPs in macrofibrils are strongly related to mechanical properties of a hair.

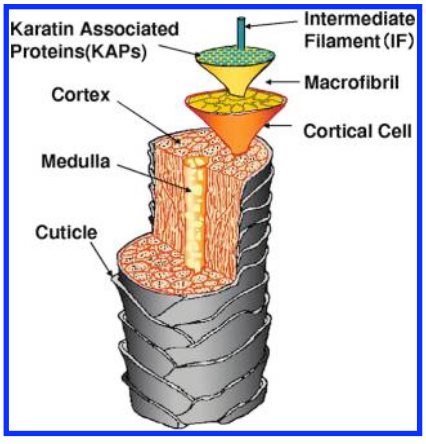

Figure 1. Structure of human hair.

Direct analytical methods to investigate protein secondary structures of hair include solid state NMR,[13] X-ray diffraction,[14−17] and vibrational spectropies.[15,18−21] Vibrational spectroscopies are widely used to analyze the composition and secondary structures of keratines. The composition and structural change of a hair due to chemical treatment, UV irradiation, physical stress, and aging have been studied by infrared and Raman spectroscopies. In particular, Raman

Received: November 13, 2011
Revised: December 31, 2011
Published: January 5, 2012

microspectroscopy is one of the most powerful methods to investigate unlabeled hairs nondestructively with high spatial resolution (approximately 1 μm).[19−21] Space-resolved Raman microspectroscopy studies of protein secondary structure in a human hair with chemical treatment[19] and aging[20] have already been reported. The conformation and orientation of proteins in an intact human hair have also been studied with polarized Raman microspectroscopy.[21] However, the long data acquisition time in these previous studies has hindered high-speed imaging studies of the protein secondary structure distribution in a hair. Since the condition of a hair can be inhomogeneously and/or rapidly changed by weathering or cosmetic treatments, it is desirable to obtain space-resolved spectral information with a high speed. Coherent anti-Stokes Raman scattering (CARS) microscopy has been a technique of focus for high-speed vibrational imaging.[22−31] However, conventional CARS microscopy using two narrow-band lasers is not suitable for protein structure studies,[29] because it provides only monochromatic image due to one particular vibrational resonance. It is known that not only the band intensity but also the peak position can change with structural changes of proteins. A full spectral profile is indispensable for obtaining molecular information on protein structures.

Recently, we have developed a multiplex CARS microspectroscopic system using an ultrabroadband laser source (white light laser source).[30] It enables us to obtain CARS spectra over the whole spectral range in the fingerprint region with short acquisition time. In a previous study, we showed that CARS microspectroscopy combined with the maximum entropy method (MEM)[32,33] is highly useful for spectral imaging of living cells with a high speed. In the present study, we apply our CARS microspectroscopic system to study protein secondary structures of intact and treated human hairs.

EXPERIMENTAL SECTION

Human Gray Hair Specimen. A human gray straight hair fiber without chemical treatments, such as permanent waving or dyeing, was collected from a healthy Japanese male (one of the authors). We chose a gray hair fiber in order to avoid the photodamage. The hair fiber was washed with a shampoo and was rinsed with ion-exchange water. After drying, the hair fiber was sliced with a microtome to yield a 5-μm-thick cross section, and the specimen was then mounted on a microscope slide glass.

Human Gray Hair with Chemical and Mechanical Treatments. A human gray hair sample without chemical treatments was collected from a healthy Japanese male. The hair sample was washed with a shampoo and was rinsed with ion-exchange water. After drying, the hair was cut into two pieces. One piece was mounted on a microscope slide glass without further treatment as a control sample. The other was soaked in 20 mL of the first agent of a commercial permanent waving product for more than 6 h to reduce disulfide bonds in the hair, and rinsed with ion-exchange water. The hair sample was then mechanically extended to be about 150% in order to induce a change of the secondary structures of proteins.[34,35] All the hair samples, soaked in polydimethylsiloxane, SH-200 (Toray Industries Inc., Tokyo, Japan) in order to improve the refractive index matching, were sandwiched with a coverslip and a microscope slide glass. Polydimethylsiloxane cannot penetrate into the hair sample due to its high molecular weight.

CARS Spectroscopic Imaging. We used the CARS microspectrometer we developed. The details of the CARS system are described elsewhere.[30] Owing to the near-infrared excitation (>1064 nm), we can detect the CARS signals of the hair samples even in the forward direction. The observed CARS spectra were intensity-corrected by a nonresonant background signal from an underneath cover glass measured under the same experimental conditions. The third-order nonlinear susceptibility $\chi^{(3)}$, whose imaginary part corresponds to ordinary (spontaneous) Raman spectra, was retrieved from the CARS spectra by the MEM.[30−33] The lateral and axial spatial resolutions were about 0.5 and 4.5 μm, respectively. Human hair has sub-micrometer-sized heterogeneous structures over an approximately 100 μm diameter. It is therefore necessary to obtain an image over several tens of μm square to include the medulla, cortex, and cuticle. In other words, 10 000 (100 × 100) pixels with 0.5 μm pitch are typically required. Owing to the capability of fast image acquisition (50 ms/pixel), the present CARS system allows us to obtain a set of vibrational images in the fingerprint region in less than 10 min.

RESULTS AND DISCUSSION

CARS Spectroscopic Imaging of a Hair Specimen. Figure 2a shows the Im[$\chi^{(3)}$] spectra obtained from two

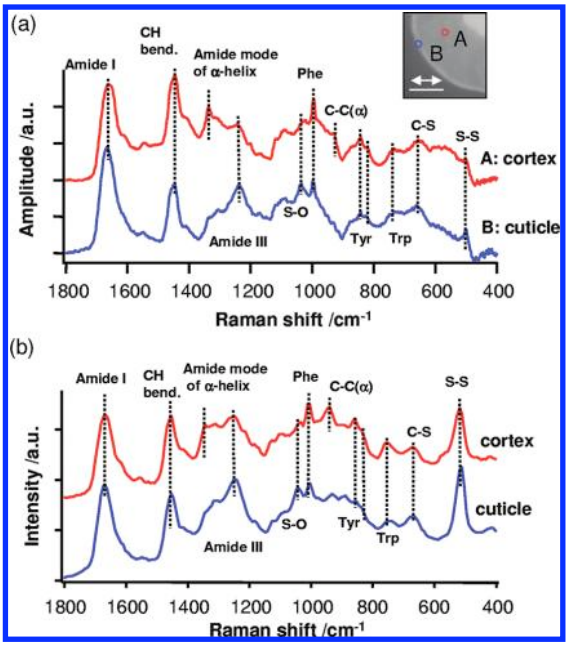

Figure 2. (a) Im[$\chi^{(3)}$] spectra of the cortex and cuticle in the hair. Each spectrum is obtained within 1 s with laser power at sample total 40 mW (1064 nm pump laser, 20 mW; ultrabroadband Stokes laser, 20 mW). The pump polarization is indicated by the double-headed arrow in the inset. (b) Spontaneous Raman spectra of a cortex and cuticle in the hair. Each spectrum is obtained within 120 s with laser power at sample 8 mW (excitation wavelength, 632.8 nm). The scale bar in the inset corresponds to 20 μm.

different positions (A and B) in the hair sample as indicated in the inset. The positions indicated as A and B correspond to cortex (fibrous materials) and cuticle (outer layer scales), respectively. For comparison, typical spontaneous Raman spectra of the cortex and cuticle regions are shown in Figure 2b. The retrieved Im[$\chi^{(3)}$] spectra (Figure 2a) agree well with the spontaneous Raman spectra (Figure 2b). The disagreement in the region below 600 cm^{-1} is due to the low sensitivity of the current CARS microspectroscopic system. It can be improved

dx.doi.org/10.1021/jp210914x | J. Phys. Chem. B 2012, 116, 1452−1457

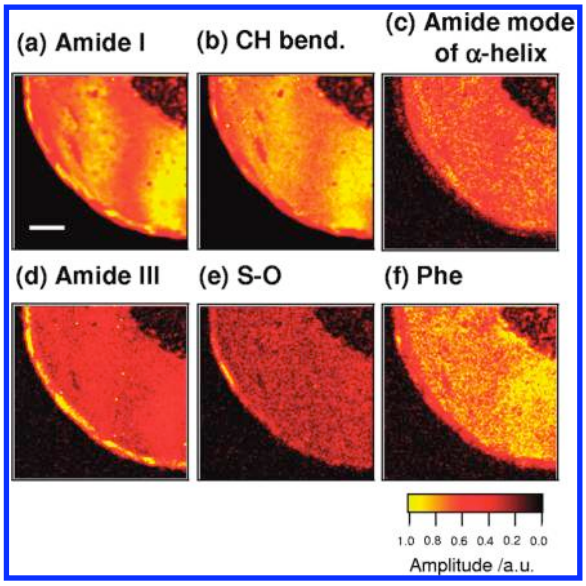

Figure 3. Multimode (6 frequencies) Im$[\chi^{(3)}]$ images of the human hair specimen. The exposure time for each pixel is 50 ms, and each image consists of 101 × 101 pixels, corresponding to 50 μm × 50 μm. Overall measurement time is approximately 10 min. The scale bar corresponds to 10 μm.

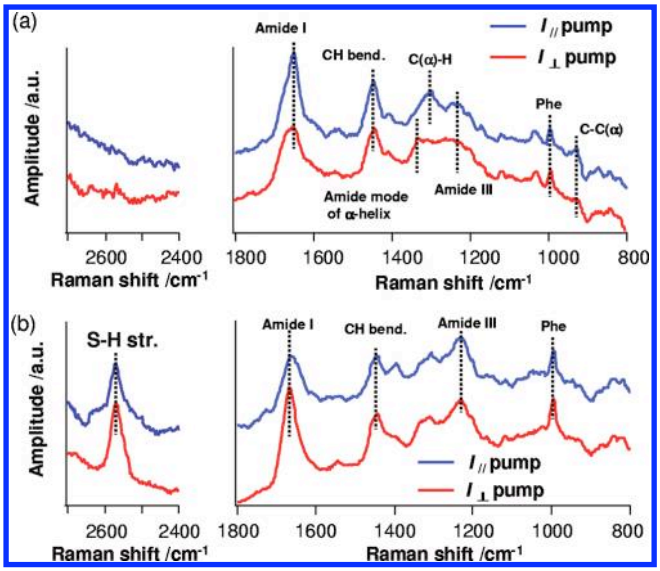

Figure 4. Polarized Im$[\chi^{(3)}]$ spectra of hair in the cortex region, (a) without and (b) with the treatments.

Table 1. Polarization Dependences of the Amplitude, Peak Position, and Band Width of the Amide I Mode

	untreated hair		treated hair	
	$I_{\parallel}$	$I_{\perp}$	$I_{\parallel}$	$I_{\perp}$
amplitude/a.u.	0.1	0.14	0.14	0.08
peak position/cm^{-1}	1656	1650	1664	1658
band width/cm^{-1}	34	30	26	35

by changing the short-pass and long-pass filters for the CARS and Stokes fields. Although the main spectral features in the two Im$[\chi^{(3)}]$ spectra originate from keratin proteins, the spectra of the cortex (A) and cuticle (B) regions are clearly different from each other. In the cortex region, the secondary structure of the protein is determined to be the α-helical structure[36,37]

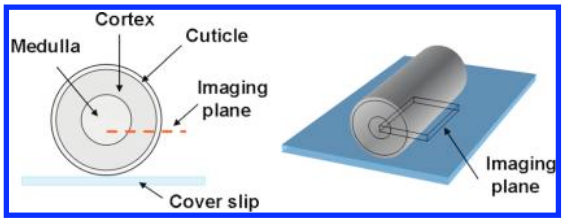

Figure 5. Schematics of the imaging plane in the hair.

from the peak positions of the amide I (1661 cm^{-1}) and III (1246 cm^{-1}) bands as well as the presence of the α-helix amide mode (1336 cm^{-1}) and the C−C(α) stretch mode (993 cm^{-1}). On the other hand, the peak positions of amide I (1666 cm^{-1}) and amide III (1238 cm^{-1}) in the cuticle region indicate that the protein secondary structure is β-sheet or random coil.[36] The strong S−O band (1036 cm^{-1}) is observed in the cuticle region. This finding is consistent with the fact that cuticle has a higher concentration of cysteic acid than other regions.[10]

Figure 3a−f shows label-free and multimode (6 frequencies) Im$[\chi^{(3)}]$ images of the untreated human hair specimen. The images include those due to amide I (a), CH bend (b), α-helix amide mode[37] (c), amide III (d), S−O (e), and phenylalanine (Phe, f), respectively. Peak heights are used for making these images. First, Figure 3a shows similar intensity distributions of amide I band in the cortex and cuticle regions. This suggests that the protein content in both regions is expected to be similar quantitatively. Second, parts c and d of Figure 3 give opposite image contrasts for the cortex and cuticle regions. In the cortex region, stronger α-helix amide mode and weaker amide III are observed compared to the cuticle. This difference in intensity distribution again reflects the fact that protein secondary structures in the cortex region are mainly α-helical and that in the cuticle they are mainly β-sheet or random structure. Third, in Figure 3f, the signal intensity at 1003 cm^{-1} is higher in the cortex region, indicating that proteins in the cortex region are rich in Phe. This result agrees well with the fact that the cortex proteins have a higher concentration of Phe.[10] Fourth, Figure 3e shows the CARS image due to the S−O stretch band. Interestingly, the S−O band intensity is higher in a particular area of the cuticle region. It is well-known that cysteic acid is generated through oxidization of cystine in hairs. Therefore, this result suggests that the oxidation process of cystine does not take place homogeneously in the cuticle region. One possible reason would be a weathering effect induced by the sunlight. Finally, no strong signal is observed in the medulla region for all vibrational frequencies in Figure 3a−f, because the media is composed of a porous structure, which works as a strong light scatterer. By using CARS microspectroscopy, we can visualize chemical heterogeneity in the hair sample as demonstrated in Figure 3.

CARS Spectra and Spectral Imaging of Hair Samples with and without Chemical and Mechanical Treatments. Figure 4 shows Im$[\chi^{(3)}]$ spectra of pieces of a hair sample in the cortex region, without (Figure 4a) and with (Figure 4b) the treatments. We apply the polarization CARS technique to both of the samples by changing the polarization of the pump laser in order to obtain information on molecular orientation in a hair. The spectral profiles indicated as $I_{\parallel}$ and $I_{\perp}$ correspond to the pump polarization parallel and perpendicular to the hair shaft, respectively.

We now focus on the polarization dependence of Im$[\chi^{(3)}]$ spectra obtained from the untreated hair sample. First,

dx.doi.org/10.1021/jp210914x | J. Phys. Chem. B 2012, 116, 1452−1457

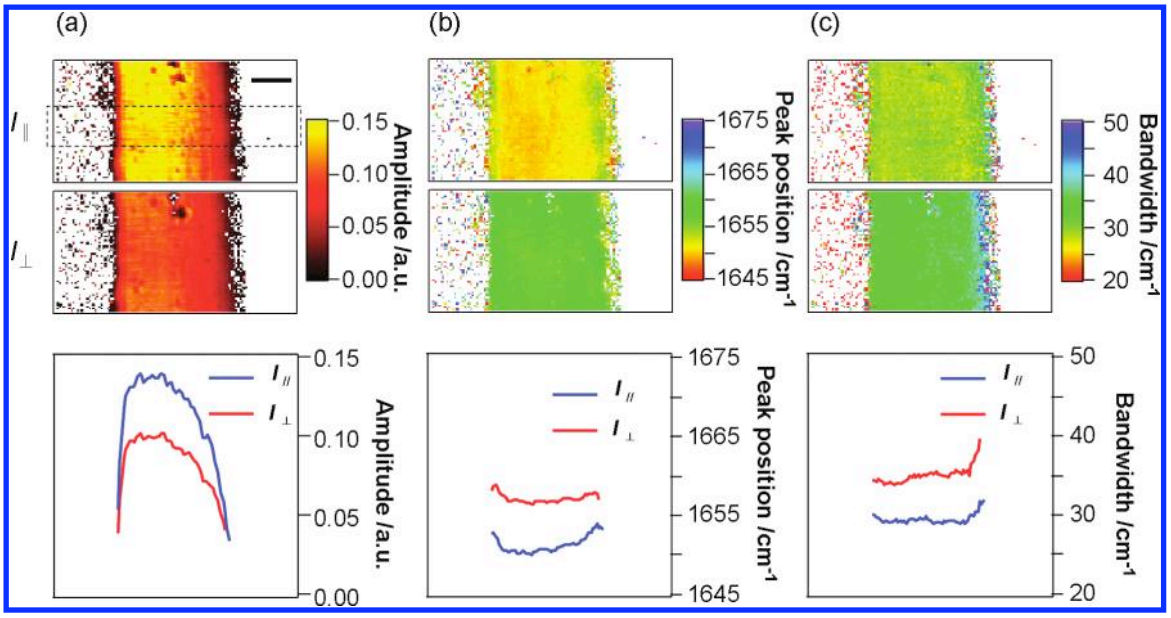

Figure 6. Intersection images of (a) the peak height, (b) the peak position, and (c) the bandwidth of the amide I band observed in the parallel and perpendicular Im[$\chi^{(3)}$] spectra of untreated hair. Only those points whose signal-to-noise ratios are higher than 3 in the peak height are included in the images. The profiles of the amplitude, the peak position, and the bandwidth are also shown beneath the corresponding images. The profiles are obtained by averaging 10 μm along the hair shaft (highlighted by a dashed line box in part a) and are plotted against the distance along the radial direction of the hair shaft. The exposure time for each pixel is 50 ms, and each image consists of 61 × 121 pixels, corresponding to 30 μm × 60 μm. Overall measurement time is approximately 7 min. The scale bar corresponds to 10 μm.

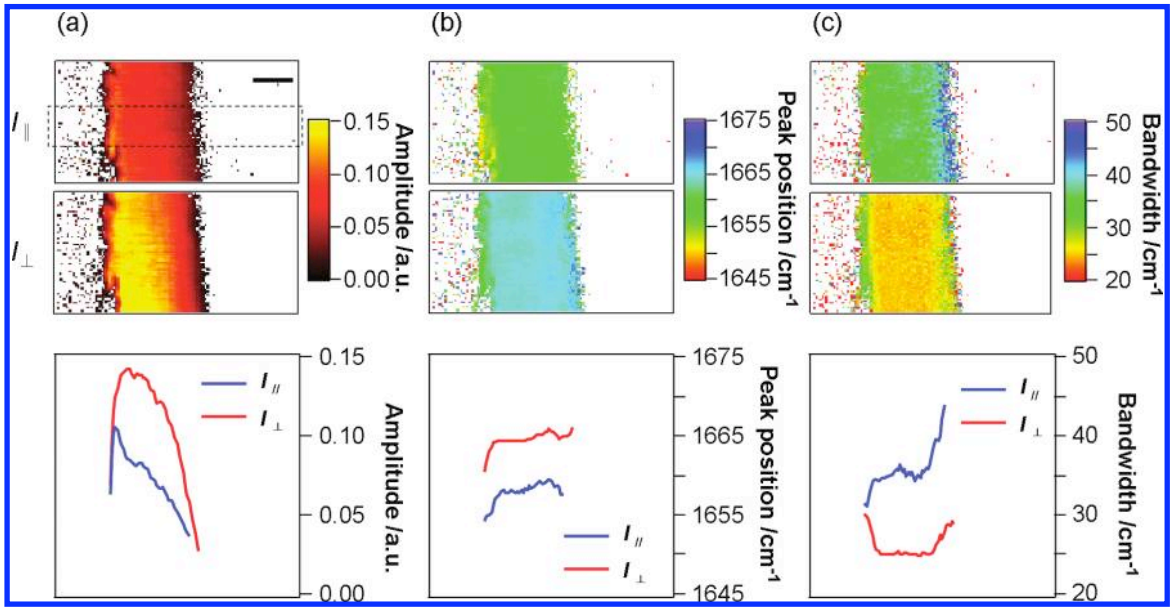

Figure 7. Intersection images of (a) the peak height, (b) the peak position, and (c) the bandwidth of the amide I band observed in the parallel and perpendicular Im[$\chi^{(3)}$] spectra of the treated hair. The experimental conditions are the same as those in Figure 6. The scale bar corresponds to 10 μm.

compared to the spectra of the cortex of the hair specimen in Figure 2a, a new extra band is found at 1304 cm^{-1} in the $I_{\parallel}$ spectrum, which is ascribed to be the C(α)−H bending mode of α-helical proteins. Second, the peak position and the bandwidth of the amide I mode in the $I_{\parallel}$ spectrum is red-shifted and narrower than those in the $I_{\perp}$ spectrum. Although the amide I band is mainly assigned to the C═O stretch mode in the amide bond,[36] the peak position and bandwidth depend on the secondary structures.[19,39] Therefore, the peak position and bandwidth of the amide I show polarization dependence. Third, the C−C(α) stretch (935 cm^{-1}) and α-helix amide mode (1341 cm^{-1}) bands are stronger and the C(α)−H bend (1304 cm^{-1}) band is weaker in $I_{\parallel}$ than in $I_{\perp}$. These three spectral features indicate that the orientation of the α-helix is parallel to the hair shaft. It is consistent with the known fact that the IFs in a straight hair are highly oriented along the hair shaft.[21] Hence, we consider that the polarization dependence primarily arises from the secondary structures.

Next, we focus on the treated hair. First, the spectral features of the treated hair are slightly different from those of the untreated sample. A new band is found at the Raman shift of 2555 cm^{-1}, which is not observed in the untreated sample. This

dx.doi.org/10.1021/jp210914x | J. Phys. Chem. B 2012, 116, 1452−1457

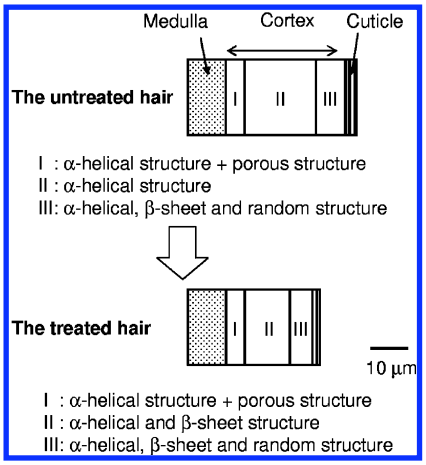

Figure 8. Proposed structures of a hair with and without the treatments.

band is assigned to the S−H stretch mode of cysteine. On the other hand, the S−O stretch (1036 cm^{-1}), which is observed in the untreated sample, is not observed in the chemically treated sample. These spectral changes confirm that the chemical reduction, which converts the S−O stretch into the S−H stretch, certainly occurs in our sample with the chemical treatment. Second, the polarization dependence of the peak position, the peak height, and the bandwidth of the amide I mode are completely different from those of the untreated sample (Table 1). The peak position and the bandwidth of the amide I mode in $I_{\parallel}$ is greatly red-shifted and broader than in $I_{\perp}$. Moreover, the amide III band (1230 cm^{-1}), which is an indicator of the β-sheet structures, becomes much stronger with the treatment. The spectral changes of the amide I mode and the appearance of the amide III band strongly suggest the protein secondary structure change from α-helix to β-sheet with the mechanical and chemical treatments. Similar structural changes have been reported on a horse hair sample,[15] a wool sample,[38] and a human hair sample.[34,35] There is no obvious characteristic peak due to α-helix in the spectra in Figure 4b. Therefore, almost all the α-helical structure should be transformed into the β-sheet.

Spatial Distributions of Protein Secondary Structures. In order to visualize the spatial distributions of protein secondary structures, we construct two-dimensional intersection images (see Figure 5) of the peak height, the peak position, and the bandwidth of the amide I band observed in the parallel and perpendicular Im$[\chi^{(3)}]$ spectra. Figure 6 shows those images of the untreated hair sample with the profiles of the peak height, the peak position, and the bandwidth. In Figure 6b, the peak position of the amide I mode is gradually blue-shifted from the inner to the outer in both the parallel and perpendicular spectra, suggesting that the ratio of the α-helical structure (lower peak position, 1645−1660 cm^{-1}) to the β-sheet (higher peak position, 1665−1680 cm^{-1}) or random structure (higher peak position, 1660−1670 cm^{-1})[36] is smaller in the outside than in the inside. From the fact that the IFs mainly consist of α-helices and KAPs of random structures, this experimental result shows that KAPs are abundant in the outside and IFs are abundant in the inside of the cortex.

From a closer examination of the profiles, it is evident that the spatial distributions of the peak position and the bandwidth can be divided into two regions: one with a small gradient in the inner part of the cortex and the other with a steep slope in the outer side. A previous small angle X-ray scattering (SAXS) proposed the existence of two structural zones, a core of highly ordered α-keratin and its surrounding zone of moderately ordered α-keratin.[14] The two different regions of the cortex found in the present study are thought to correspond to these two zones. We estimate the core size to be approximately 20 μm. Such information on the core size was not obtainable with SAXS because of low spatial resolution. In addition, small changes of the peak position and the bandwidth are found even in the core itself, indicating that protein structure in the core is not homogeneous.

Next, we discuss the profiles of the treated hair shown in Figure 7. More drastic changes in the spatial distributions of the peak position and the bandwidth are observed in the treated hair than in the untreated. Three layers are more clearly observed especially in the bandwidth profiles. The layer closest to the medulla is newly found. The two inner layers including the new one correspond to the core and the outer layer of the surrounding zone. The peak position in the new layer is still 1650−1655 cm^{-1} (α-helical) as in the case of the untreated hair, while that in the other two areas is 1660−1670 cm^{-1} (β-sheet and random coil), reflecting the treatment induced structural changes from the α-helical structure to the β-sheet or random coil. This finding implies that the response of the newly found layer to the mechanical extension is different from those of the other two layers of the cortex. These varied responses to the mechanical extension can be explained as follows. Only the cortex region attached to the medulla can have a porous structure because the medulla is composed of a porous structure. Namely, this layer can be considered as the transition layer between the medulla and the cortex. This porous structure in the cortex close to the medulla is thought to play a role to relax the mechanical extension of the IFs. As a result, the IFs in the cortex close to the medulla suffer less stress than the IFs in the other part of the cortex, which are not associated with a porous structure and change their protein structures by the mechanical extension.

On the basis of the experimental results shown above, we propose a three-layered structure model of cortex as shown in Figure 8. The newly found first layer is located at the boundary between the cortex and the medulla, whose thickness is a few micrometers. In this layer, the IFs circumvent the phase transition of proteins by the mechanical extension owing to its porous structure. The second layer is located in the middle region of the cortex. This layer is the main part of the cortex, and its thickness is approximately 20 μm. The third layer is located at the boundary between the cortex and the cuticle, whose thickness is several micrometers. This layer has abundant of proteins with the β-sheet and/or random structures.

■ CONCLUSIONS

We obtained multimode Im$[\chi^{(3)}]$ images of untreated and treated human hairs in the fingerprint region by using CARS microspectroscopic system with a nanosecond white light laser source. The Im$[\chi^{(3)}]$ images show inhomogeneous chemical compositions and protein secondary structures in the hair. The polarization-resolved measurement enables us to obtain information about molecular orientation in the hair. The results obtained from the untreated and treated hairs clearly show the treatment induced changes of the protein secondary structures from the α-helical structure to the β-sheet or random coil. On the basis of the peak position and the bandwidth

dx.doi.org/10.1021/jp210914x | J. Phys. Chem. B 2012, 116, 1452−1457

profiles of the amide I band, we propose a three-layered structure model of cortex.

AUTHOR INFORMATION

Corresponding Author

*E-mail: hhama@chem.s.u-tokyo.ac.jp.

ACKNOWLEDGMENTS

This work was partly supported by the SENTAN project (Program-S) of the Japan Science and Technology Agency (JST). H. K. gratefully acknowledges financial support from Grand-Aid for Scientific Research on Priority Areas "Molecular Science for Supra Functional Systems" [477] from MEXT and the Precursory Research for Embryonic Science and Technology (PRESTO) program of JST. The authors thank LEUKOS Company for technical support with the dual-output supercontinuum laser source. The authors gratefully acknowledge Dr. T. Wakisaka, Dr. K. Kita, Mr. H. Sato, and Mr. M. Oguri (Kao Corporation, Ltd.) for their fruitful discussion. We gratefully acknowledge Mr. J. Ukon (HORIBA, Ltd.) for assisting in the collaboration between the Japanese and French groups.

REFERENCES

(1) Bear, R. S. *J. Am. Chem. Soc.* **1944**, *66*, 1297−1305.
(2) Bear, R. S. *J. Am. Chem. Soc.* **1944**, *66*, 2043−2050.
(3) Greenfield, N. J. *Nat. Protoc.* **2006**, *1*, 2876−2890.
(4) Whitmore, L.; Wallance, B. A. *Biopolymers* **2008**, *89*, 392−400.
(5) Wishart, D. S.; Sykes, B. D.; Richards, F. M. *Biochemistry* **1992**, *31*, 1647−1651.
(6) Wishart, D. S.; Sykes, B. D. *J. Biomol. NMR* **1994**, *4*, 171−180.
(7) Surewicz, W. K.; Mantsch, H. H.; Chapman, D. *Biochemistry* **1993**, *32*, 389−394.
(8) Carey, P. R. *Annu. Rev. Phys. Chem.* **2006**, *57*, 527−554.
(9) Kinalwa, M. N.; Ewan., W. B.; Doig, A. J. *Anal. Chem.* **2010**, *82*, 6347−6349.
(10) Robbins, C. R. *Chemical and Physical Behavior of Human Hair*, 4th ed.; Springer-Verlag: New York, 2002.
(11) Feughelman, M. *J. Appl. Polym. Sci.* **2002**, *83*, 489−507.
(12) Hearle, J. W. S. *Int. J. Biol. Macromol.* **2000**, *27*, 123−138.
(13) Nishikawa, N.; Tanizawa, Y.; Tanaka, S.; Horiguchi, Y.; Asakura, T. *Polymer* **1998**, *39*, 3835−3840.
(14) Busson, B.; Engtrom, P.; Doucet, J. *J. Synchrotron Radiat.* **1999**, *6*, 1021−1030.
(15) Kreplak, L.; Doucet, J.; Dumas, P.; Briki, F. *Biophys. J.* **2004**, *87*, 640−647.
(16) Nagase, S.; Kajiura, Y.; Mamada, A.; Abe, H.; Shibuichi, S.; Satoh, N.; Itou, T.; Shinohara, Y.; Amemiya, Y. *J. Cosmet. Sci.* **2009**, *60*, 637−648.
(17) Kajiura, Y.; Watanabe, S.; Itou, T.; Nakamura, K.; Iida, A.; Inoue, K.; Yagi, N.; Shinohara, Y.; Amemiya, Y. *J. Struct. Biol.* **2006**, *155*, 438−444.
(18) Rintoul, L.; Carter, E. A.; Stewart, S. D.; Fredricks, P. M. *Biopolymers* **2000**, *57*, 19−28.
(19) Kuzuhara, A. *Biopolymers* **2005**, *77*, 335−344.
(20) Kuzuhara, A.; Fujiwara, N.; Hori, T. *Biopolymers* **2007**, *87*, 134−140.
(21) Ackermann, K. R.; Koster, J.; Schlücker, S. *J. Biophotonics* **2008**, *1*, 419−424.
(22) Zumbusch, A.; Holtom, G. R.; Xie, X. S. *Phys. Rev. Lett.* **1999**, *82*, 4142−4145.
(23) Hashimoto, M.; Araki, T.; Kawata, S. *Opt. Lett.* **2000**, *25*, 1768−1770.
(24) Cheng, J.-X.; Xie, X. S. *J. Phys. Chem. B* **2004**, *108*, 827−840.
(25) Potma, E. O.; Xie, X. S.; Muntean, L.; Preusser, J.; Jones, D.; Ye, J.; Leone, S. R.; Hinsberg, W. D.; Schade, W. *J. Phys. Chem. B* **2004**, *108*, 1296−1301.
(26) Kano, H.; Hamaguchi, H. *Anal. Chem.* **2007**, *79*, 8967−8973.
(27) Freudiger, C. W.; Min, W.; Saar, B. G.; Lu, S.; Holtom, G. R.; He, C.; Tsai, J. C.; Kang, J. X.; Xie, X. S. *Science* **2008**, *322*, 1857−1861.
(28) Kox, M. H. F.; Domke, K. F.; Day, J. P. R.; Rago, G.; Stavitski, E.; Bonn, M.; Weckhuysen, B. M. *Angew. Chem., Int. Ed* **2009**, *48*, 8990−8994.
(29) Zimmerley, M.; Lin, C.-Y.; Oertel, D. C.; Marsh, J. M.; Ward, J. L.; Potma, E. O. *J. Biomed. Opt.* **2009**, *14*, 044019.
(30) Okuno, M.; Kano, H.; Leproux, P.; Couderc, V.; Day, J. P. R.; Bonn, M.; Hamaguchi, H. *Angew. Chem., Int. Ed.* **2010**, *49*, 6773−6777.
(31) Day, J. P. R.; Domeke, K. F.; Rago, G.; Kano, H.; Hamaguchi, H.; Vartiainen, E. M.; Bonn, M. *J. Phys. Chem. B* **2011**, *115*, 7713−7725.
(32) Vartiainen, E. M. *J. Opt. Soc. Am. B* **1990**, *7*, 722−725.
(33) Vartiainen, E. M.; Rinia, H. A.; Müller, M.; Bonn, M. *Opt. Express* **2006**, *14*, 3622−3630.
(34) Wong, M.; Wis-Surel, G.; Epps, J. *J. Soc. Cosmet. Chem.* **1994**, *45*, 347−352.
(35) Ogawa, S.; Fujii, K.; Kaneyama, K.; Arai, K.; Joko, K. *J. Cosmet. Sci.* **2000**, *51*, 379−399.
(36) Carey, P. R. *Biochemical Applications of Raman and Resonant Raman Spectroscopies*; Academic Press: New York, 1982.
(37) Tsuboi, M.; Suzuki, M.; Overman, S. A.; Thomas, G. J. Jr. *Biochemistry* **2000**, *39*, 2677−2684.
(38) Bendit, E. G *Nature* **1957**, *179*, 535.
(39) Tsuboi, M.; Kaneuchi, F.; Ikeda, T.; Akahane, K. *Can. J. Chem.* **1991**, *69*, 1752−1757.